High resolution three-dimensional photoacoustic imaging of human finger joints in vivo

Lei Xi and Huabei Jiang

Citation: Applied Physics Letters **107**, 063701 (2015); doi: 10.1063/1.4926859
View online: http://dx.doi.org/10.1063/1.4926859
View Table of Contents: http://scitation.aip.org/content/aip/journal/apl/107/6?ver=pdfcov
Published by the AIP Publishing

High resolution three-dimensional photoacoustic imaging of human finger joints *in vivo*

Lei Xi[1,a)] and Huabei Jiang[1,2,a)]
[1]*School of Physical Electronics, University of Electronic Science and Technology of China, Chengdu, Sichuan, China*
[2]*Department of Biomedical Engineering, University of Florida, Gainesville, Florida 32611, USA*

(Received 10 May 2015; accepted 3 July 2015; published online 11 August 2015)

We present a method for noninvasively imaging the hand joints using a three-dimensional (3D) photoacoustic imaging (PAI) system. This 3D PAI system utilizes cylindrical scanning in data collection and virtual-detector concept in image reconstruction. The maximum lateral and axial resolutions of the PAI system are 70 μm and 240 μm. The cross-sectional photoacoustic images of a healthy joint clearly exhibited major internal structures including phalanx and tendons, which are not available from the current photoacoustic imaging methods. The *in vivo* PAI results obtained are comparable with the corresponding 3.0 T MRI images of the finger joint. This study suggests that the proposed method has the potential to be used in early detection of joint diseases such as osteoarthritis. © *2015 AIP Publishing LLC*. [http://dx.doi.org/10.1063/1.4926859]

Arthritis is the leading cause of disability in the population over 50-year old and affects millions of people over the world.[1] There are two common types of arthritis: osteoarthritis (OA) and rheumatoid arthritis (RA). According to a clinical survey, half of the people over 50-year old suffer from OA that results in swelling, stiffness, and pain of distal interphalangeal (DIP) joints, proximal interphalangeal (PIP) joints, ankles, knees, and shoulders.[1] Currently, early-stage diagnosis and subsequent optimized treatment offer the best protection of both the joint structures and functions. Most OA patients have symptoms in DIP joints in the early stage. However, current clinical imaging techniques such as x-ray computed tomography (CT), magnetic resonance imaging (MRI), and ultrasound imaging (US) have limitations for early diagnosis of OA in DIP joints. X-ray is insensitive to soft tissues and has ionizing radiation.[2] The high cost as well as low temporal resolution of MRI prevents it from being widely used in OA patients, especially in the developing countries.[2] US is used to evaluate the thickness of articular cavity, which commonly changes in intermediate and advanced stages.[2]

Numerous recent studies have shown that optical imaging technique has the potential to become an effective tool for early diagnosis of OA in the finger joint. Yuan and Hielscher used volumetric diffuse optical tomography (DOT) to recover both optical absorption and scattering coefficients of joint tissues to evaluate the finger joints. However, due to the highly scattering nature of joint tissues, the spatial resolution is insufficient in the clinical use.[3,4] Hence, Yuan *et al*. proposed to improve the spatial resolution of DOT by utilizing prior structural information of X-ray tomosynthesis to guide the quantitative reconstruction of DOT. However, the ionizing radiation of X-ray is still a major safety concern.[3] Photoacoustic imaging (PAI), which combines rich optical contrast and excellent spatial resolution of ultrasound, presents noninvasive and nonionizing imaging of tumors, blood vessels, and finger joints with promising penetration depth.[5–9] Wang *et al*. used 2D photoacoustic computed tomography to visualize subcutaneous tissue, phalanx inside the DIP joint in a hand amputated from a female cadaver.[10] Sun *et al*. applied the finite-element-based quantitative reconstruction algorithm in a spherical-scanning-based PAI system to reconstruct structures and functional parameters of *in vivo* finger joints.[11] Ultrasound array coupled with multiple optical fiber bundles were developed to image blood vessels in the fingers.[12–14] Even previous studies are exciting, but none of them provides high-resolution PA images of phalanx and tendons of human finger joints *in vivo*. Here, we propose to utilize virtual-detector concept, which was previously used to solve the problem of limited directivity of transducers in 2D PAI,[15,16] to volumetrically reconstruct phalanx and tendons of DIP joints with high spatial resolution.

The schematic of the imaging interface is shown in Fig. 1(a). The laser beam emitted from a tunable Ti:Sapphire laser (Surelite I-20, Continuum, CA) with 6 nanosecond (ns)

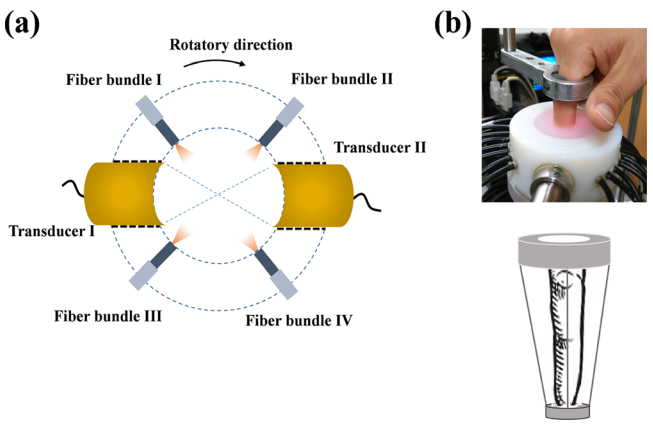

FIG. 1. (a) Schematic of the PAI system. (b) PAI-joint interface for DIP joint imaging.

[a)]Author to whom correspondence should be addressed. Electronic addresses: hjiang@bme.ufl.edu and xilei1985@uestc.edu.cn

duration and 20 Hz repetition rate was equally split and then coupled into four optical fiber bundles via beam splitter cubes and convex lenses. The laser beams delivered by the fiber bundles illuminated the surface of the finger and provided a uniform light distribution in the imaging plane. The wavelength of the laser was tuned to 720 nm in the near infrared (NIR) window to enable good penetration depth into the articular tissues. The measured pulse energy from each fiber bundle was 3.5 mJ resulting in 2.8 mJ/cm^2 on the surface of the finger, which was far below the ANSI safety limit of 22 mJ/cm^2. The generated wideband photoacoustic signals were detected by two acoustic transducers (V320-SU, Olympus, MA), which were positioned symmetrically in the imaging plane. The diameter, central frequency, and focal length of these transducers were 19 mm, 7.5 MHz, and 25.1 mm. After the amplifier (5073PR, Olympus, MA), the photoacoustic signals were recorded by a 12 bits data acquisition card (NI5124, National Instruments Corporation, TX) with a sampling rate of 50 MHz. All the components were fixed in a resinic mode, and the imaging area was filled with water-intralipid mixed solution to couple the photoacoustic signals. The whole imaging interface was mounted on a rotator and scanned 120 steps with a constant interval of 1.5° to cover a 360° receiving angle. The finger was immobilized in the center of imaging area via an aluminum ring and three plastic optical fibers (Fig. 1(b)). Since the fibers were transparent and thin, the influence on illumination and detection was negligible. For 3D data collection, the whole imaging interface was axially scanned 50 steps with an interval of 240 μm. The total experimental time was 5 min.

In conventional cylindrical-scanning-based photoacoustic imaging systems, flat transducers are commonly utilized to collect the acoustic signals where the axial resolution is primarily dependent on the transducer's size as well as the radius of the scanning circle. High axial resolution requires ultrasmall transducers. However, the sensitivity of the transducer is positively proportional to the active area of the transducer and determines the signal-to-noise (SNR) ratio of the system as well as the image quality. Hence, we employed focused transducers in data collection and applied virtual-detector concept in image reconstruction to gain both high sensitivity and high axial resolution in this cylindrical-scanning-based photoacoustic imaging system.

Fig. 2 shows the schematic of 3D acoustic field distribution of a typical self-focusing transducer as well as the way to collect 3D photoacoustic data. The size of the focal point is determined by the following equation:

$$R_{(-6\,\mathrm{dB})} = 1.028FC/fD, \tag{1}$$

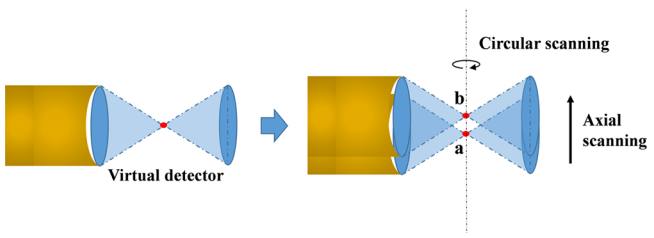

FIG. 2. Schematic of the virtual detector concept used in image reconstruction and the cylindrical scanning in data collection.

where C, f, F, and D represent the sound velocity, the central frequency, the focal length, and the diameter of the transducer. The maximum axial resolution of our system was calculated to be 240 μm. A modified delay and sum algorithm was developed to reconstruct the images where we used the scanning center as the coordinate origin and adjusted the time delay of the signal to accommodate the spatial difference between the virtual detector and the transducer's surface.

Several phantom experiments were conducted to evaluate the performance of the system. To test the lateral resolution, we embedded a metal wire with a diameter of 50 μm in a solid tissue mimicking phantom with an optical absorption coefficient of 0.01 mm^{-1} and a reduced scattering coefficient of 1.0 mm^{-1}. As shown in Fig. 3(a), the system could accurately recover the position and shape of the wire. However, the imaged size (Fig. 3(b)) is 70 μm, which determines the maximum lateral resolution of this system. In conventional photoacoustic computed tomography systems, the limited directivity of flat acoustic transducers may lead to imbalanced image quality, which degrades from the imaging center to the edge. A knotted human hair and eight 0.7 mm pencil leads were embedded in the same tissue mimicking phantom and imaged separately by the system. From the results shown in Figs. 3(c) and 3(d), we found that there was no deterioration in an active imaging area of 5.5 mm in radius. However, when the targets were located outside the active imaging area, the imaging quality descended quickly (see the imaged pencil leads indicated by red arrows in Fig. 3(d)). The active imaging area is determined by the effective focal zone of the focused transducer, which was measured to be 5.5 mm in this system.

After the phantom evaluation, we imaged 4 healthy DIP joints of middle fingers in 2 female and 2 male human hands. Fig. 4(a) shows the positions of selected imaging planes and

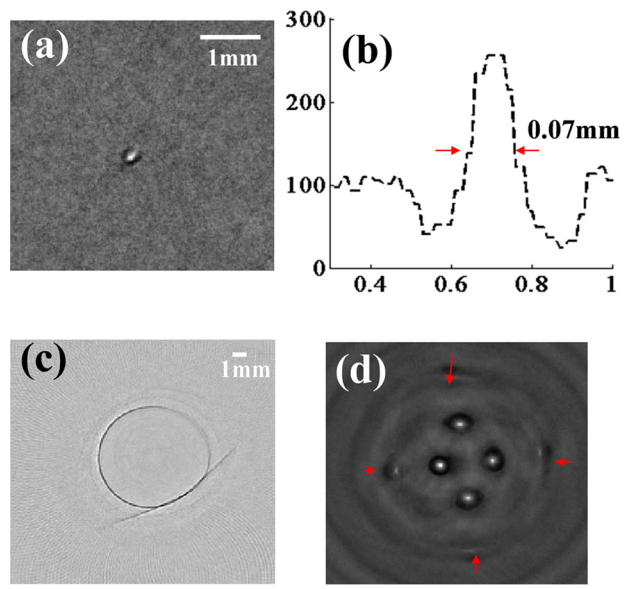

FIG. 3. (a) A typical cross-sectional photoacoustic image of a metal wire. (b) Quantitative analysis of the imaged size of the metal wire. (c) The image result of a knotted human hair embedded in a tissue mimicking phantom. (d) A selected cross-sectional image of eight 0.7 mm pencil leads.

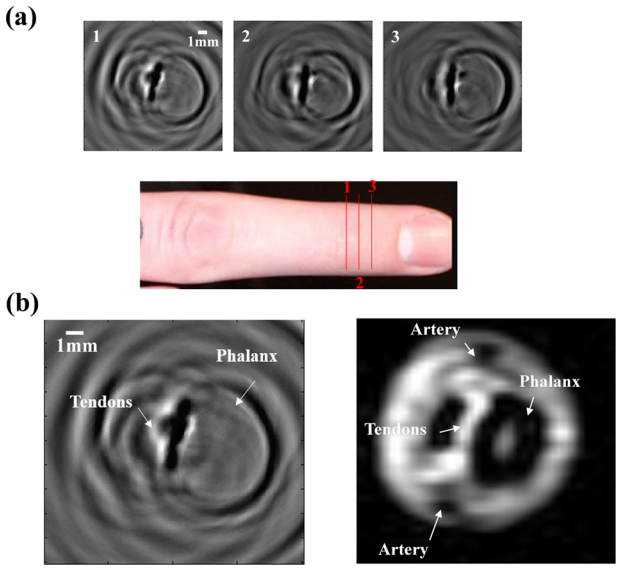

FIG. 4. (a) Four selected cross-sectional images and stack of all slices of DIP joints in a female middle finger. (b) Comparison between the photoacoustic image and the corresponding MRI image. (Multimedia view) [URL: http://dx.doi.org/10.1063/1.4926859.1]

corresponding photoacoustic images. We can clearly recognize the tendons and phalanx in the DIP joints with high resolution. In addition, as shown in Fig. 4(a), the structural difference between different imaging planes was well identified inside the active imaging area. However, we found that the arteries in the joints were not well imaged due to severe deformation outside the active imaging area. This could be solved by choosing different transducers with larger active focal zones in the future. In Fig. 4(b), we compared the photoacoustic image with its corresponding MRI image. We found that the major structures in the photoacoustic image agreed well with those in the MRI image, indicating that the resolution of our system is comparable with 3.0 T MRI for imaging of finger joints.

In sum, we proposed and built a cylindrical-scanning-based 3D photoacoustic imaging system by utilizing focused transducers coupled with the concept of virtual detector for high resolution imaging of finger joints. Through both theoretical calculations and phantom experiments, the maximum spatial resolution of this system is 70 μm in lateral and 240 μm in axial. We have demonstrated the feasibility of this system in noninvasive imaging of major structures in the DIP joints with sufficient penetration depth and resolution. As a promising complement to conventional screening and diagnostic technologies such as ultrasound, MRI, and X-ray CT, the proposed method may effectively contribute to the clinical diagnosis of finger joint arthritis with its high optical contrast and possibility of using various optical contrast agents. Additionally, this method has the potential to offer functional imaging ability using multi-wavelength strategy.[17,18] However, there are still several improvements that need to be undertaken. First, the motion of finger joints during the experiments leads to the degradation of the image quality, which could be overcome by utilizing multiple transducers and high-repetition laser sources. For instance, if we use 8 transducers and a commercially available pulsed laser with a repetition rate of 100 Hz, the total experimental time will be reduced to 15 s. Second, current active imaging area is confirmed due to the fixed focal length of transducers. However, through employing the liquid-based acoustic lens with variable focal length in our previous studies,[19,20] we can easily change the size of active imaging area depending on specific applications. Third, due to heterogeneous sound velocities of joint tissues, current linear reconstruction algorithm assuming that the sound velocity is a constant leads to some image artifacts. In the next step, finite-element based quantitative reconstruction algorithm that can be used to derive functional parameters of joint tissues will be employed to solve this problem.[21]

We thank Lei Yao for the assistance in developing the reconstruction algorithm. This work was sponsored in part by the J. Crayton Pruitt Family Endowment Fund (Jiang) and a startup grant (A03012023601011) by University of Electronic Science and Technology of China (Xi).

[1]F. W. Roemer and A. Guermazi, Osteoarthritis Cartilage **22**(12), 2003 (2014).
[2]F. W. Roemer, M. D. Crema, S. Trattnig, and A. Guermazi, Radiology **260**(2), 332 (2011).
[3]Z. Yuan, Q. Zhang, H. Jiang, E. Sobel, and H. Jiang, Biomed. Opt. Express **1**(1), 74 (2010).
[4]A. H. Hielscher, A. D. Klose, A. K. Scheel, B. Moa-Anderson, M. Backhaus, U. Netz, and J. Beuthan, Phys. Med. Biol. **49**(7), 1147 (2004).
[5]L. V. Wang and S. Hu, Science **335**(6075), 1458 (2012).
[6]P. Beard, Interface Focus **1**(4), 602 (2011).
[7]L. Xi, S. Grobmyer, L. Wu, R. Chen, G. Zhou, L. G. Gutwein, J. Sun, W. Liao, Q. Zhou, H. Xie, and H. Jiang, Opt. Express **20**(8), 8726 (2012).
[8]L. Xiang, B. Wang, L. Ji, and H. Jiang, Sci. Rep. **3**, 1113 (2013).
[9]S. Yang, D. Xing, Q. Zhou, L. Xiang, and Y. Lao, Med. Phys. **34**(8), 3294 (2007).
[10]X. Wang, D. L. Chamberland, and D. A. Jamadar, Opt. Lett. **32**(20), 3002 (2007).
[11]Y. Sun, E. Sobel, and H. Jiang, J. Biomed. Opt. **14**(6), 064002 (2009).
[12]P. van Es, S. K. Biswas, H. J. Bernelot Moens, W. Steenbergen, and S. Manohar, J. Biomed. Opt. **19**(6), 060501 (2014).
[13]C. Lutzweiler, R. Meier, E. Rummeny, V. Ntziachristos, and D. Razansky, Opt. Lett. **39**(14), 4061 (2014).
[14]G. Xu, J. R. Rajian, G. Girish, M. J. Kaplan, J. B. Fowlkes, P. L. Carson, and X. Wang, J. Biomed. Opt. **18**(1), 010502 (2013).
[15]L. Nie, Z. Guo, and L. V. Wang, J. Biomed. Opt. **16**(7), 076005 (2011).
[16]C. Li and L. V. Wang, J. Biomed. Opt. **14**(2), 024047 (2009).
[17]J. Xiao, L. Yao, Y. Sun, E. Sobel, J. He, and H. Jiang, Opt. Express **18**(14), 14359–14365 (2010).
[18]H. Ammari, E. Bossy, V. Jugnon, and H. Kang, SIAM Rev. **52**(4), 677–695 (2010).
[19]C. Song, L. Xi, and H. Jiang, J. Appl. Phys. **114**(19), 194703 (2013).
[20]C. Song, L. Xi, and H. Jiang, Opt. Lett. **38**(15), 2930 (2013).
[21]Z. Yuan, Q. Wang, and H. Jiang, Opt. Express **15**(26), 18076–18081 (2007).